The Next-Generation Massively Parallel Reactive Flow and Transport Code PFLOTRAN: Application to CO_2 Storage in Saline Aquifers

P. Lichtner[α] (PI: lichtner@lanl.gov), C. Lu[σ], G. Hammond[β], B. Philip[α], D. Moulton[α], R. Mills[γ], B. Smith[δ], A. Valocchi[ε], K. Nakshatrala[ε], S. Yabusaki[β]

[α]Los Alamos National Laboratory,[β]Pacific Northwest National Laboratory,[γ]Oak Ridge National Laboratory,[δ]Argonne National Laboratory,[σ]University of Utah,[ε]University of Illinois at Urbana-Champaign

Abstract

The next-generation multiphase-multicomponent reactive flow and transport code PFLOTRAN is currently being developed under a SciDAC-2 project entitled: Modeling Multiscale-Multiphase-Multicomponent Subsurface Reactive Flows using Advanced Computing. PFLOTRAN is a parallel multiphase flow and multicomponent reactive transport model written from the ground up employing PETSc data structures and solvers for its parallel framework. The code employs domain decomposition for parallelization and implements an efficient parallel I/O through HDF5. It is written in a highly modular, object-oriented style in Fortran 90 and uses modern constructs such as derived types, pointers, and linked lists. Recently, PFLOTRAN has been run on a one billion node real-world problem (Hanford 300 Area) as proof-of-concept for petascale computing. It ran successfully on 1024 cores on ORNL's Jaguar Cray XT3 computer. The code has also demonstrated a relative parallel efficiency of 79% at 12,000 cores based on a strong-scaling study performed with a similar 500 million node problem executed on 3,000-12,000 cores. PFLOTRAN is currently being applied to investigate sequestration of CO_2 in various geologic media including depleted oil reservoirs and saline aquifers as a possible solution to reduce green house gas emissions. Dissolution of supercritical CO_2 in formation brines is considered an important storage mechanism to prevent possible leakage. Accurate prediction of the plume dissolution rate and migration is essential. Analytical analysis and numerical experiments have demonstrated that convective instability (Rayleigh instability) has a crucial effect on the dissolution behavior and subsequent mineralization reactions. Global stability analysis indicates that a certain grid resolution is needed to capture the features of density-driven fingering phenomena. For 3-D field scale simulations, high resolution leads to large numbers of grid nodes, unfeasible for a single workstation. In this study, we investigate the effects of convective instability on geologic sequestration of CO_2 by taking advantage of parallel computing using PFLOTRAN. The onset, development and long-term fate of a supercritical CO_2 plume will be resolved with high-resolution numerical simulations to investigate the rate of plume dissolution caused by fingering phenomena.

1. Introduction

- Sequestration of CO_2 in subsurface geologic formations containing saline aquifers could provide permanent storage for a major greenhouse gas and thereby help to mitigate global climate change.
  - Saline aquifers have an estimated world-wide storage capacity for CO_2 of 320-10,000 Gt CO_2 (Bachu, 2002).
  - A typical scenario is injection into a relatively deep saline aquifer above the critical point where CO_2 exists as a supercritical fluid (T_{crit}=31.04°C, p_{crit}=73.82 bar).
  - As supercritical CO_2 is injected into the aquifer it becomes buoyant because of its lower density compared to the brine and begins to rise, possibly eventually reaching the ground surface (Pruess, 2006). A low permeability zone or caprock may trap the CO_2 so that it can gradually dissolve into the surrounding brine.
  - As the CO_2 dissolves into the brine, the brine becomes heavier and begins to sink resulting in density-driven convection which can lead to instabilities resulting in the formation of CO_2 concentrated brine fingers protruding downward.
  - The areal extent of the plume can have an important effect on accidental release of CO_2 to the surface through abandoned bore holes and faults. The areal extent is controlled by competition between the rate of spreading of the plume and the rate at which it dissolves into the brine. Convective mixing can result in much more rapid dissipation of the supercritical CO_2 plume compared to diffusive processes alone.
  - It is important to understand the properties of the aquifer which determine the size and onset of fingering during the convective mixing process.
- Analyses of density instability of CO_2 in deep saline aquifers can be used to investigate the onset of convective mixing during CO_2 sequestration in isotropic and anisotropic porous media (Ennis-King and Paterson, 2003; Xu et al., 2006)

2. The Massively Parallel Reactive Flow and Transport Code PFLOTRAN

- The computer code PFLOTRAN solves a coupled system of mass and energy conservation equations for a number of phases including H_2O, supercritical CO_2, and black oil, and a gaseous phase. PFLOTRAN describes coupled thermal-hydrologic-chemical (THC) processes in variably saturated, nonisothermal, porous media in one (1D), two (2D), or three (3D) spatial dimensions.
- The multiphase partial differential equations solved by PFLOW for mass and energy conservation can be summarized as (Lichtner et al., 1996):

$$\frac{\partial}{\partial t}\left(\phi \sum_\alpha s_\alpha \psi_i^\alpha\right) + \nabla \cdot \sum_\alpha \left[\mathbf{q}_\alpha \rho_\alpha X_i^\alpha - \phi s_\alpha D_\alpha \rho_\alpha \nabla X_i^\alpha\right] = Q_i^\alpha, \tag{1a}$$

and

$$\frac{\partial}{\partial t}\left(\phi \sum_\alpha s_\alpha \rho_\alpha U_\alpha + (1-\phi)\rho_r c_r T\right) + \nabla \cdot \left[\mathbf{q}_\alpha \rho_\alpha H_\alpha - \kappa \nabla T\right] = Q_e. \tag{1b}$$

In these equations, α designates a phase (e.g. H_2O, supercritical CO_2, g), species are designated by the subscript i (e.g. $w = H_2O$, $c = CO_2$), ϕ denotes porosity of the geologic formation, s_α denotes the saturation state of the phase; X_i^α denotes the mole fraction of species i; ρ_α, H_α, U_α refer to the molar density, enthalpy, and internal energy of each fluid phase, respectively; $\mathbf{q}_\alpha$ denotes the Darcy flow rate defined by

$$\mathbf{q}_\alpha = -\frac{k k_{r_\alpha}}{\mu_\alpha}\nabla\left(p_\alpha - W_\alpha \rho_\alpha g \mathbf{z}\right), \tag{2}$$

where k refers to the water saturated permeability, k_{r_α} denotes the relative permeability, μ_α denotes the fluid viscosity, W_α denotes the formula weight, and g denotes the acceleration of gravity. The source/sink terms Q_i^α and Q_e, describe injection and extraction at wells. The density ρ_α of fluid phase α appearing in Eqns. (1a) and (1b) refers to the density of the fluid mixture. Use of ideal mixing for the system H_2O-CO_2 leads to a lower density of the mixture. In this work the correlation developed by Garcia (2001) is used which gives a greater mixture density in agreement with experiment. Finally, a Henry's law relation from Duan and Sun (2003) is used to compute the equilibrium concentration of CO_2 dissolved in H_2O of the form

$$X_i^\beta = K_{i,\beta\alpha} X_i^\alpha, \tag{3}$$

with Henry constant $K_{i,\beta\alpha}$, with i=CO_2, α=$CO_{2(w)}$, and β=H_2O.

- The multicomponent reactive transport equations solved by PFLOTRAN have the form (Lichtner et al., 1996):

$$\frac{\partial}{\partial t}\left(\phi \sum_\alpha s_\alpha \psi_j^\alpha\right) + \nabla \cdot \sum_\alpha \Omega_j^\alpha = -\sum_m \nu_{jm} I_m, \tag{4}$$

for the jth primary species, and

$$\frac{\partial \phi_m}{\partial t} = \bar{V}_m I_m, \tag{5}$$

for the mth mineral.

- Definitions: ψ_j^α, Ω_j^α denote the total concentration and flux, defined by the expressions

$$\psi_j^\alpha = \delta_{ij} C_j^\alpha + \sum_i \nu_{ji} C_i^\alpha, \quad \Omega_j^\alpha = (-\tau \phi s_\alpha D_\alpha \nabla + \mathbf{q}_\alpha)\psi_j^\alpha, \tag{6}$$

where C_j^α denotes the solute concentration in phase α, C_i^α denotes the concentration of the ith secondary species, related to the concentration of primary species through the mass action equations

$$C_i^\alpha = (\gamma_i^\alpha)^{-1} K_i^\alpha \prod_j \left(\gamma_j^\alpha C_j^\alpha\right)^{\nu_{ji}}, \tag{7}$$

where γ_j^α denotes the activity coefficient, and K_i^α denotes the equilibrium constant for the reaction.

- Partitioning CO_2 between H_2O and supercritical CO_2 is accomplished with the reaction

$$CO_{2(aq)} \rightleftharpoons CO_{2(g)}, \tag{8}$$

where the subscript (g) refers to the supercritical phase and (aq) to the aqueous phase. Other reactions not included above that may also significantly impact CO_2 sequestration are ion exchange and surface complexation reactions since these reactions could affect the concentrations of relevant cations such as Ca^{2+} and Mg^{2+}.

3. Parallel Implementation

- PFLOTRAN is written from the ground up to run on massively parallel computer architectures (Hammond et al., 2005, 2007; Lu and Lichtner, 2007; Mills et al., 2007).
- PFLOTRAN makes use of object-oriented features in Fortran 90 and is essentially platform independent, running on any machine that PETSc runs on. This includes laptop computers, workstations, and massively parallel high performance computing facilities. See flow diagram for PFLOTRAN shown in Figure 1. The realization-level-patch grid structure for implementing structured AMR and multilevel solvers is illustrated in Figure 2.
- Parallelization is implemented through the PETSc parallel library developed at Argonne National Laboratory (Balay et al., 1997).
  - PETSc provides a user friendly set of routines for solving systems of nonlinear equations in parallel using domain decomposition [Figure 3(a)].
  - PETSc includes parallel solvers and preconditioners, parallel construction of the Jacobian matrix and residual function, and seamless message passing, which together provide a high parallel efficiency.
  - PETSc (latest version 2.3.3) has achieved a high level of maturity that allows rapid development with efficient parallel implementation for solving large systems of non-linear partial differential equations.

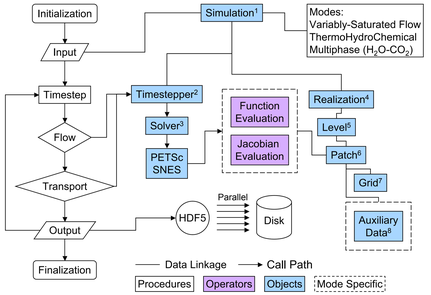

Figure 1: *PFLOTRAN flow diagram illustrating use of procedures, operators, objects, and mode specific operators and objects.*

- Flow Chart Definitions
  1. Simulation object: Highest level data structure providing all information for running a simulation
  2. Timestepper object: Pointer to Newton-Krylov solver and tolerances associated with time stepping
  3. Solver object: Pointer to nonlinear Newton and linear Krylov solvers (PETSc SNES/KSP/PC) along with associated convergence criteria
  4. Realization object: Pointer to all discretization and field variables associated with a single realization of a simulation
  5. Level object: Pointer to discretization and field variables associated with a single level of grid refinement within a realization
  6. Patch object: Pointer to discretization and field variables associated with a subset of grid cells within a level
  7. Grid object: Pointer to discretization within a patch
  8. Auxiliary Data object: Pointer to field variables within a patch

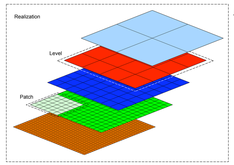

Figure 2: *Realization-level-patch grid structure used in PFLOTRAN for implementing AMR and multilevel solvers.*

- Key PFLOTRAN features/capabilities either implemented or currently being implemented (*)
  - Object-oriented data structures
  - PETSc solvers/preconditioners
  - Modular linkage to physicochemical processes
  - Collective parallel I/O through HDF5
  - AMR*
  - Multicontinuum subgrid model*
  - Multiphase flow
  - Thermal transport
  - Multicomponent transport
  - Biogeochemistry

Strong scaling results are shown in Figure 3(b) for modest sized problems running on MPP2 at PNNL/EMSL and Jaguar at ORNL (Mills et al., 2005). The benchmark problems were run on both the MPP2 cluster at PNNL/EMSL, a cluster of 1960 1.5 GHz Itanium 2 processors with Quadrics QsNetII interconnect, and Jaguar, the 5294 Opteron processor Cray XT3 at ORNL/NCCS. PFLOTRAN scales quite well on both machines, bottoming out at around 1024 processors on MPP2, and scaling exceptionally well on Jaguar, displaying linear speedup all the way up to 2048 processors, and still displaying good speedup when going from there to 4096 processors. Transport (PTRAN) was run only on MPP2 and shows similar scaling to flow (PFLOW).

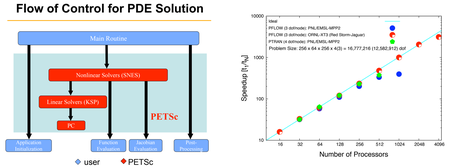

Figure 3: *(a) PETSc provides message passing capabilities, solvers and preconditions for parallel computing (left). The user supplies the residual function and Jacobian. (b) Performance of PFLOTRAN (PFLOW refers to flow and PTRAN to reactive transport) (right) running a single phase thermo-hydrologic benchmark problem on a $256\times64\times256$ grid with three and four degrees of freedom per node, respectively (approximately 12.6 and 16.8 million degrees of freedom total).*

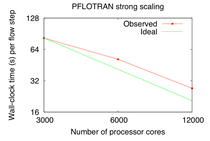

Figure 4: *(a) Strong scaling speedup curve for 500 million node problem run on Jaguar.*

One-billion node performance on Jaguar

# procs	newton its	bcgs its	time(sec)
1024	16	1697	1143
2048	16	1626	697
4096	16	1720	325

Figure 4: *(b) Jaguar performance for one billion node problem.*

Figure 4(a) shows the wall-clock time versus the number of processor cores for a 500 million node problem run on Jaguar at ORNL using dual-core processors. Scaling is reasonable and the slight reduction in performance is attributed to load imbalance due to the use of inactive nodes in the calculation. Recently, PFLOTRAN has been run on a one billion node ($4096\times2048\times128$ = 1,073,741,824 nodes), real-world problem (Hanford 300 Area) as proof-of-concept for petascale computing. Timing for a single step are presented in Figure 4(b).

4. Convective Mixing

4.1 PFLOTRAN Simulations

Two 3D simulations are presented involving a coarse and fine grid for a sandstone host rock containing calcite cement (Lu and Lichtner, 2007). In both simulations an isotropic permeability of 2×10^{-12} m^2 is used with a porosity of 15%. The nominal temperature and pressure is 50°C and 200 bars. The computational domain is 250 m thick and 7×7 km in lateral extent. CO_2 is injected at a depth of 50 m below the top of the domain. No flow boundary conditions are imposed at the top, bottom, front and back of the domain with constant pressure at the left and right sides. An injection rate of 1 Mt/y for 20 years was used in the simulations. This corresponds to roughly 75% of the CO_2 produced by a 1000 MW gas-fired power plant in 20 years.

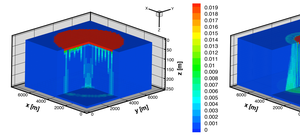

Figure 5: *(a) Coarse grid.* **Figure 5:** *(b) Fine grid.*

Shown in Figure 5 is the dissolved CO_2 mole fraction corresponding to an elapsed time of 300 years calculated on a coarse-grid with $40\times40\times25$ nodes. The grid spacing is 175 m horizontally and 10 m vertically. In Figure 5 the grid is refined in the x and y directions by a factor of 4 with the same grid spacing in the z direction. In the find grid simulation 128 processors were used. For both simulations the finger width is equal to the horizontal grid spacing indicating that convergence is not obtained. Indeed, for the parameters used in the simulations according to stability analysis, the critical wavelength should be on the order of $\lambda_c = 0.05$ m and $\tau_c = 6.2\times10^{-4}$ y. This is much too small to resolve even with the fastest computers using a uniform grid.

In Figure 6(a) the total moles of CO_2 is plotted as a function of time for both coarse and fine grids showing the amount of CO_2 dissolved in the brine and as supercritical CO_2. The supercritical phase disappears at approximately 400 years for the fine grid compared to 800 years for the coarse grid. A slight increase in total CO_2 occurs due to the dissolution of calcite cement resulting from carbonic acid produced by injection of supercritical CO_2.

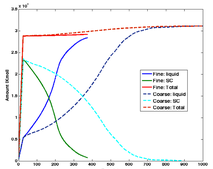

Figure 6: *Supercritical, aqueous and total CO_2 plotted as a function of time for coarse and fine grids.*

Shown in Figures 7(a) and 7(b) are the pH and calcite volume fraction after an elapsed time of 1000 years. The pH is lower in the region containing elevated CO_2 concentrations. Very little reaction with calcite occurs within the formation except at the top where high CO_2 concentrations persist.
The effect of temperature on the reaction instability is illustrated in Figures 8 and 9 where T = 50°C, 150°C and 250°C. At higher temperature the mixture density becomes less than the brine density and the dissolved CO_2 rises.

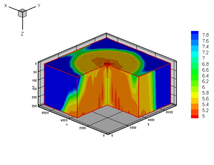

Figure 7: *(a) pH after 1000 years.* **Figure 7:** *(b) Calcite volume fraction after 1000 years.*

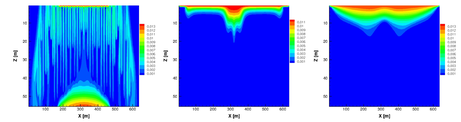

Figure 8: *Calculated dissolved CO_2 profiles at different temperatures of 50°C, 162°C and 200°C from left to right for a 3m NaCl brine as the mixture density varies from greater, to equal, to less than the brine density.*

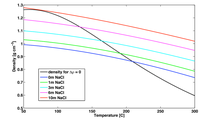

Figure 9: *Mixture density as a function of temperature based on the Garcia (2001) correlation based on non-ideal mixing. The quantity $\Delta\rho$ denotes the difference in mixture and brine densities.*

5. Conclusion

- PFLOTRAN's objected-oriented structure provides a flexible and modular framework for adding additional capabilities for scientific applications.
- PFLOTRAN was demonstrated to scale to one-billion nodes on 1024 processors, run on Jaguar at ORNL, as proof-of-concept for petascale computing.
- The calculated rate of dissolution of CO_2 into the formation brine of a saline aquifer in which supercritical CO_2 is injected was found to be highly dependent on grid resolution because of density-driven instabilities resulting in fingering of the dissolved CO_2.
- According to stability analysis, finger width can range over many orders of magnitude and for highly permeable regions may be too small to resolve even with massively parallel computing architectures.
- Numerical experiments utilizing massive parallel computing can provide the basis for formulating such upscaling relations.

Acknowledgments

This research is supported by the U.S. Department of Energy's Office of Science under the Scientific Discovery through Advanced Computing (SciDAC) program. Computing time was provided by a 2007 DOE INCITE award for the project: *Modeling Reactive Flows in Porous Media.*

References

[1] Bachu, S. (2002) Sequestration of CO_2 in geological media in response to climate change: road map for site selection using the transform of the geological space into the CO_2 phase space. *Energy Convers. Manag.* **43** 87–102.

[2] Balay, S., W.D. Gropp, L.C. McInnes and B.F. Smith (1997) Efficient Management of Parallelism in Object Oriented Numerical Software Libraries, Modern Software Tools in Scientific Computing, Ed. E. Arge, A.M. Bruaset and H.P. Langtangen, 163-202, Birkhauser Press.

[3] Duan. Z. and R. Sun (2003) An improved model calculating CO_2 solubility in pure water and aqueous NaCl solutions from 273 to 533 K and from 0 to 2000 bar, *Chem. Geol.* **193** 257–271.

[4] Ennis-King, J. and L. Paterson (2003) Role of convective mixing in the long-term storage of carbon dioxide in deep saline formations. In: SPE annual technical conference and exhibition, SPE 84344, Denver colorado.

[5] Garcia, J.E. (2001) Density of aqueous solutions of CO_2, Technical Report LBNL-49023, Lawrence Berkeley National Laboratory, Berkeley, CA.

[6] Hammond, G.E., A.J. Valocchi, P.C. Lichtner (2005) Application of Jacobian-free NewtonKrylov with physics-based preconditioning to biogeochemical transport, Adv. Wat. Res., 28, 359–376.

[7] Lichtner, P.C. 1996 Continuum Formulation of Multicomponent-Multiphase Reactive Transport, In: *Reactive Transport in Porous Media* (eds. P.C. Lichtner, C.I. Steefel, and E.H. Oelkers), *Reviews in Mineralogy*, **34**, 1–81.

[8] Lu, C, P.C. Lichtner (2007) High resolution numerical investigation on the effect of convective instability on long term CO2 storage in saline aquifers, J. Phys. Conference Series, 78, 012042 doi:10.1088/1742-6596/78/1/012042.

[9] Mills, R.T., C. Lu, and P.C. Lichtner (2005) PFLOTRAN: A massively parallel simulator for reactive flows in geologic media, SC2005.

[10] Pruess, K. (2006). On leakage from geological storage reservoirs of CO_2, Proceedings, International Symposium on Site Characterization for CO2 Geological Storage, Lawrence Berkeley National Laboratory, Berkeley, CA, 178–181.

[11] Xu, X., S. Chen and D. Zhang (2006) Convective stability analysis of the long-term storage of carbon dioxide in deep saline aquifers, *Adv. Wat. Res.* **29** 397–407.